Indonesian Journal of Electrical Engineering and Computer Science
Vol. 39, No. 1, July 2025, pp. 669~680
ISSN: 2502-4752, DOI: 10.11591/ijeecs.v39.i1.pp669-680

Non-contact breathing rate monitoring using infrared thermography and machine learning

Anadya Ghina Salsabila[1], Rachmad Setiawan[1], Nada Fitrieyatul Hikmah[1], Zain Budi Syulthoni[2]
[1]Department of Biomedical Engineering, Faculty of Intelligent Electrical Technology and Informatics, Institut Teknologi Sepuluh Nopember (ITS), Surabaya, Indonesia
[2]Medical Profession Study Program, Faculty of Medicine and Health, Institut Teknologi Sepuluh Nopember (ITS), Surabaya, Indonesia

Article Info

Article history:

Received Aug 9, 2024
Revised Mar 13, 2025
Accepted Mar 26, 2025

Keywords:

Breathing rate
Health
Infrared thermography
Machine learning
Non-contact measurement

ABSTRACT

Monitoring vital physiological parameters such as breathing rate (BR) is crucial for assessing patient health. However, current contact-based measurement methods often cause discomfort, particularly in infants or burn patients. This study aims to develop a non-contact system for monitoring BR using infrared thermography (IRT). This approach permits to detects and tracks the nose from thermal video, extracts temperature variations into a breathing signal, and processes this signal to estimate BR. The estimated BR is then classified into three health categories (bradypnea/normal/tachypnea) using k-nearest neighbors (k-NN). To evaluate system accuracy and robustness, experiments were conducted under three conditions: (i) stationary breathing, (ii) breathing with head movements, and (iii) specific breathing patterns. Results demonstrated high consistency with contact-based photoplethysmography (PPG) measurements, achieving complement of the absolute normalized difference (CAND) index values of 94.57%, 93.71%, and 96.06% across the three conditions and mean absolute BR errors of 1.045 bpm, 1.259 bpm, and 0.607 bpm. The k-NN classifier demonstrated high performance with training, validation, and testing accuracies of 100%, 100%, and 99.2%, respectively. Sensitivity, specificity, precision, and F-measure results confirm system reliability for non-contact BR monitoring in clinical and practical settings.

Corresponding Author:

Nada Fitrieyatul Hikmah
Department of Biomedical Engineering, Faculty of Intelligent Electrical and Informatics Technology
Institut Teknologi Sepuluh Nopember (ITS)
Surabaya, Indonesia
Email: nadafh@bme.its.ac.id

1. INTRODUCTION

Monitoring vital physiological parameters such as breathing rate (BR) is crucial for assessing patient health. BR, defined as the number of breathing cycles per minute, includes inspiration (inhaling oxygen) and expiration (exhaling carbon dioxide) [1]. Abnormal BR (tachypnea, bradypnea, or apnea) can serve as an early indicator of various respiratory diseases, including asthma, chronic obstructive pulmonary disease (COPD), and pulmonary thromboembolism [2], [3]. Despite its importance, BR is often undocumented due to the lack of accessible monitoring methods [4]. Current techniques typically require the attachment of sensors to the patient's body, which can cause discomfort, stress, and even pain, particularly in children and burn patients [5].

Traditional BR monitoring methods involve assessing chest movements with respiratory belt transducers, electrical impedance, ECG, PPG morphology, capnography, or spirometry [6]-[10]. While these methods are reliable, they are intrusive and may lead to sensor dislocation, which could compromise measurement accuracy or, in individuals with sensitive skin like infants or burn victims, cause irritation or even skin damage. Additionally, using disposable sensors, such as electrodes, increases complexity and costs, presents challenges in handling and hygiene, and contributes to medical waste [11]. Consequently, there is a growing demand for non-contact BR monitoring alternatives that improve patient comfort and optimize medical resources [12].

Several non-contact techniques have been proposed, such as audio analysis, doppler radar, magnetic induction, and imaging methods using RGB cameras an thermal imaging [13]-[16]. Each method has its limitations, including sensitivity to ambient noise, subject position constraints, high sensitivity to motion artifacts, and lighting conditions [17]. Thermal imaging, or infrared thermography (IRT), offers significant advantages due to its non-contact, non-invasive, and non-radiative nature, and does not require light, making it usable day and night [11], [12]. IRT is a technology that detects infrared radiation emitted by an object, converts it into temperature values, and generates a thermal image representing the temperature distribution [18]. Shaikh *et al.* [19] demonstrated that respiration data obtained via IRT shows no significant difference compared to data from respiratory inductance plethysmography, highlighting IRT as an effective, non-contact method for monitoring human respiration.

IRT-based breathing function measurement relies on temperature differences observed in the nasal area during breathing cycles [19]. Abbas *et al.* [16] developed an algorithm to monitor the BR by analyzing temperature fluctuations around the nostrils [16]. Lewis *et al.* [20] employed IRT to observe temperature variations across the nostrils, accounting for different breathing patterns, including spontaneous, slow, and rapid breathing. The data collected from the thermal camera were primarily obtained under optimal conditions, characterized by minimal head movements and normal breathing [16], [19], [20]. In contrast, this study evaluates the effectiveness of our method in more challenging scenarios, such as head movements and breathing disorders. We evaluated the robustness of our approach in the presence of motion artifacts and assessed its accuracy and reliability across different breathing patterns.

Lewis *et al.* [20] significantly advanced the use of IRT for obtaining the BR by tracking the nostrils with a Piecewise Bezier Volume Deformation model, while Jin Fei and Ioannis Pavlidis employed a network of probabilistic trackers to segment and track the nostrils [7]. However, these methods required manual selection of the region of interest (ROI) in the initial frame [7], [20], [21]. Moreover, tracking algorithms faced various challenges, such as failures during sudden or large head movements or when the subject opened their mouth, which often caused the breathing signal to have zero values [19], [20]. To address these challenges, this study utilizes a Haar Cascade classifier to automatically detect and track the nose region in thermal video, combined with a canny edge detector for nostril detection to enhance accuracy. An interpolation algorithm was also applied to prevent signal loss during tracking failures, which would otherwise result in zero-value signals. This interpolation method repairs the extracted signals, representing an innovative approach that has not been addressed in prior studies.

Pereira *et al.* [12] applied a bandpass Butterworth filter to enhance the signal-to-noise ratio (SNR) of the breathing signal. Similarly, Ioannis Pavlidis employed a lowpass Butterworth filter to improve SNR and introduced a method for characterizing breathing patterns by calculating the mean dynamic breathing signal and identifying breathing cycles uding zero-cross thresholding [7]. Jagadev and Giri made a significant contribution in classifying the breathing signal using machine learning by using a k-nearest neighbour (k-NN) classifier to determine whether the subject exhibit normal or abnormal respiration or is specifically experiencing Bradypnea or Tachypnea [2]. In this study, we applied the Butterworth bandpass filter to reduce noise and enhance the SNR of the obtained breathing signal. After that, we implemented peak detection to automatically identify the breathing cycles in the filtered breathing signals and calculate the breaths per minute (BPM) value, thereby overcoming the limitations present in prior studies [7], [16], [19], [20], which necessitated manual intervention for the determination of BPM. Futhermore, we classified the breathing signals into three categories: bradypnea, normal, and tachypnea, using the k-NN algorithm.

This study introduces a novel and reliable approach for contactless monitoring of BRs using thermal imaging. In contrast to other techniques that require manual selection of the ROI [7], [20], [21], this approach automatically detects the nose in the initial frame. We also use a canny edge detector to detect nostrils to make a more accurate and applied interpolation algorithm to prevent the zero value of breathing signal caused by missing ROI. While previous research validated their algorithms under optimal conditions with minimal head movements and normal breathing [16], [19], [20], we evaluate ours in more challenging situations, such as head movements and breathing disorders. Additionally, we employed machine learning, using a 10-fold cross-validation k-NN classifier, to classify breathing conditions and determine whether the person has normal breathing or conditions like bradypnea (slow breathing) or tachypnea (fast breathing). This system is expected to yield valuable insights into the application of thermal imaging for BR detection and present a promising non-contact alternative for healthcare professionals.

2. METHOD

This section offers a detailed overview of the sequential steps involved in the effective monitoring of BR, as illustrated in Figure 1. The process begins with data acquisition using an infrared thermal camera, followed by ROI detection and tracking. Subsequent steps include ROM detection, breathing signal extraction, and filtering. The extracted BR values are then classified into bradypnea, normal, and tachypnea using a k-NN classifier.

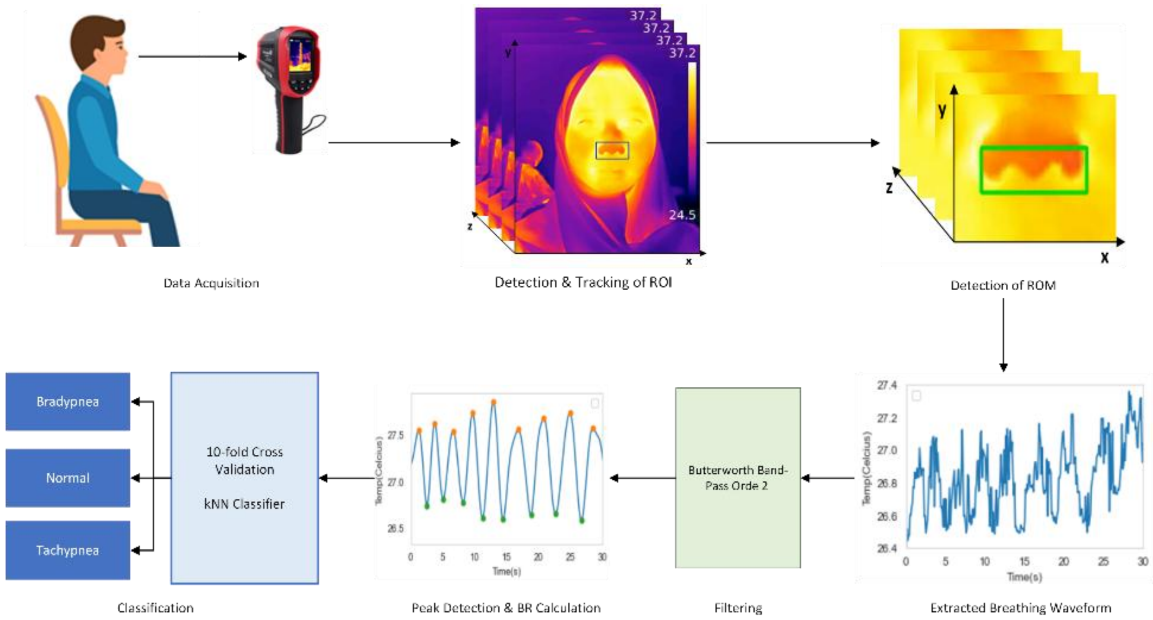

Figure 1. Overview of the system design

2.1. Data acquisition

The experiments were conducted in the laboratorium room, where the temperature was controlled at 24°C. The study involved ten volunteer participants, comprising males and females aged 18–25 years. They were seated comfortably and the IR camera connected to a laptop was positioned parallel to their faces. The data acquisition process is illustrated in Figure 2, showing Figure 2(a) the thermal imager and Figure 2(b) the experimental setup. The thermal imager used was the UTi260B model [22].

The camera was placed 0.25 meters from the subject, focusing exclusively on the facial area. Data was collected under three different conditions: (1) the subject was instructed to remain still and breathe normally, (2) the subject breathed normally while performing some head movements, and (3) the subject simulated deep, slow breathing (bradypnea) or shallow, rapid breathing (tachypnea). Videos were recorded at a frame rate of 10 Hz for 60 seconds per condition.

(a) (b)

Figure 2. Data acquisition (a) thermal imager used and (b) experimental setup

2.2. Detection and tracking of ROI

This approach relies on the temperature changes around the nostrils during the breathing cycle (inspiration and expiration). As cool air is inspired from the environment and warm air is expired from the lungs, IRT can precisely detect these temperature variations, as shown in Figure 3. To calculate the BR from the thermal video, the nose (ROI) must be automatically detected in the initial frame.

The first step was face segmentation using the multi-level Otsu's method [23]. In 1979, Nobuyuki Otsu [24] introduced an image thresholding technique based on clustering, allowing the division of an image into two categories: background and foreground. This algorithm employs discriminant analysis to determine the optimal threshold value (T*) by minimizing *within-class variance* (σ_W^2) or, alternatively, maximizing *between-class variance* (σ_B^2), as defined by (1),

$$T^* = arg \max_{1 \le T < L} \{\sigma_B^2(T) = \sigma^2(T) - \sigma_W^2(T)\}, \tag{1}$$

where σ^2 denotes the total variance, T represents the threshold value, and L corresponds to the gray levels. This equation can be further elaborated into (2),

$$\sigma_B^2(T) = \omega_1(T)[\mu_1(T) - \mu]^2 + \omega_2(T)[\mu_2(T) - \mu]^2. \tag{2}$$

here, ωi represents the probabilities of the two classes (background and foreground), μ denotes the mean intensity of the original image, and μi refers to the mean intensity of each respective class. Specifically, 1 and 2 correspond to classes C1 and C2, respectively.

Multi-level Otsu's method was applied for face segmentation to effectively separate the subject's face from the background, minimizing background noise that can affect detection accuracy in thermal imaging. This step ensures that only the largest region in the binary image corresponds to the face. After segmentation, the Haar Cascade classifier was used to detect the nose region within the segmented face. Haar Cascade is well-known for its efficiency in detecting facial features in digital images, even when objects are at different scales and orientations, making it suitable for this task [25]. Previous studies, such as those by Setjo and Faridah [26], have also demonstrated the effectiveness of this method in thermal imaging. By combining Otsu's segmentation and Haar Cascade, our approach aimed to improve the accuracy and reliability of nose detection in thermal videos.

2.3. Identification of region of measurement

In order to improve the SNR, a second and smaller ROI that focuses on the area around the nostrils, namely the Region of Measurement (ROM), is determined. ROM is identified for each tracked ROI by considering the nose edges and is found using the canny edge detector [26]. The nostril region, where temperature fluctuations occur during breathing, was then segmented. These temperature values were tracked over time, allowing us to extract the breathing signal based on the temperature changes associated with inspiration and expiration.

2.4. Extraction of breathing signal and signal processing

The breathing signal extraction according to the average temperature value $\bar{s}(t)$ of the ROM for each frame is given by (3),

$$\bar{s}(t) = \frac{1}{mn} \sum_{i=0}^{m-1} \sum_{j=0}^{n-1} s(i, j, t), \tag{3}$$

where $s(i, j, t)$ represents the temperature at pixel (i, j) at time t, m is the width of the ROM, and n is its length. In (3) describes the process of extracting the breathing signal from thermal images by using the average temperature in the ROM for each image frame. The average temperature $\bar{s}(t)$ at time t is calculated by summing the temperatures at each pixel $s(i, j, t)$ within the ROM and dividing by the total number of pixels (mn).

The extracted breathing signal undergoes post-processing to improve its quality and reduce noise. Due to difficulties in tracking the ROI in thermal video, not all acquired breathing signals display optimal morphology. When the nostrils are undetected, the signal may register as zero, leading to discontinuities. To resolve this issue, an interpolation algorithm replaces zero values by averaging the immediate neighboring values, effectively restoring continuity in the signal. Since the breathing signal typically has a low SNR-affected by factors such as emissivity variations, camera response, temperature calibration, atmospheric conditions, and environmental reflections-a second-order Butterworth band-pass filter is applied, with 3 dB cutoff frequencies between 0.1 Hz and 0.5 Hz, to isolate the respiratory signal range and enhance clarity by attenuating background noise. After filtering, peak detection is performed to identify the breathing cycles within the signal, which enables the calculation of BR in subsequent steps.

2.5. Breathing rate calculation

The BR is calculated from the filtered breathing signal by counting the number of peaks in the signal profile, where the peaks correspond to expirations and the crests indicate inspirations. A complete breath cycle consists of one peak and one crest, and the total number of these cycles in a minute gives the BR. To evaluate the accuracy of the detected BR in comparison to the photoplethysmography (PPG) ground truth, the complement of the absolute normalized difference (CAND) index is computed, with a higher CAND value signifying better detection of vital signs. The CAND value is determined using (4):

$$CAND = 1 - \frac{|GT - TI|}{GT}, \tag{4}$$

where GT represents the actual BR values obtained from PPG and TI represents the result obtained using the thermal imaging-based BR detection system.

2.6. Classification using k-NN

The k-NN classifier, a non-linear supervised learning method, categorizes breathing signals into tachypnea, normal, and bradypnea without assuming data distribution. Using majority voting among its k-NN, it assigns unknown attributes to the dominant class [27]. The formulation of this algorithm in the training phase is defined by (5):

$$y = f(z), \tag{5}$$

where z is a vector containing the extracted features, and y represents the class (Normal, Tachypnea, or Bradypnea) that z belongs to. In the testing phase, the classifier assigns classes to new instances according to (6):

$$y_q = f(z_q), \tag{6}$$

where z_q represents the vector of query features, and y_q is the predicted class (Normal, Tachypnea, or Bradypnea) for z_q. The k in k-NN refers to the number of nearest neighbors used to classify a test sample. Choosing the right value for k is crucial, as it significantly impacts the performance of the k-NN classifier. The goal is to find a balance between overfitting and underfitting.

A total of 416 60-second breathing signals were sourced from the BIDMC PPG and respiration dataset [28] and an SQLite-driven database [29] for training the k-NN classifier, comprising 90 bradypnea signals, 200 normal breathing signals, and 126 tachypnea signals. The extracted features from these breathing signals included BPM and the count of normal and abnormal breaths within each signal, which were then input into the k-NN classifier. The dataset, containing both normal and abnormal breathing signals, is mathematically represented as shown in (7):

$$D_n = \left\{ (z_i, y_i)_{i=1}^{n} | z_i \in \mathbb{R}^d, y_i \in \{Normal, Tachypnea, Bradypnea\} \right\}, \tag{7}$$

where D_n represents the dataset comprising of vectors z_i and y_i, wherein z_i contains the BPM, number of normal and abnormal breath cycles in each signal, and y_i identifies the class to which z_i belongs.

The dataset was initially split 7:3 for training and testing. The training dataset was further divided into a training set and a validation set using the cross-validation method. The training set contains data samples used for building the model, while the validation set holds back samples to evaluate the model's performance. Cross-validation, a statistical method to assess a machine learning model's accuracy on unseen data, typically involves the following steps:

a) Randomly shuffle the dataset.
b) Split the dataset into n groups, commonly 5 or 10.
c) Each sample is used once and for model training n-1 times in the validation set.

In this study, n was set to 10. The training data was randomly divided into 10 folds of approximately equal size. The first fold was used as the validation set, while the model was trained on the remaining 9 folds. This 10-fold cross-validation process generated 10 results, with the final result being their average. The testing dataset, consisting of breathing signals, was used to evaluate the final model's performance and was kept separate until the model was fully developed.

The robustness and effectiveness of the k-NN classifier were assessed by calculating its training, validation, and testing accuracies. Furthermore, performance metrics such as sensitivity, specificity, precision, and F-measure were calculated for each class individually. The mathematical expressions used for these calculations are provided in (8) to (11),

$$Sensitivity = \frac{TP}{TP+FN}, \tag{8}$$

$$Specificity = \frac{TN}{TN+FP}, \tag{9}$$

$$Precision = \frac{TP}{TP+FP}, \tag{10}$$

$$F - Measure = 2 \times \frac{Precision \times Sensitivity}{Precision + Sensitivity}, \tag{11}$$

where true positive (TP) refers to when subjects with normal breathing were correctly classified as normal, false positive (FP) refers to when subjects with normal breathing were wrongly classified as tachypnea/bradypnea, true negative (TN) refers to when normal subjects were correctly classified as not having tachypnea/bradypnea, and false negative (FN) refers to when unhealthy subjects (tachypnea/bradypnea) were wrongly classified as having normal breathing.

3. RESULTS AND DISCUSSION

This section provides a summary of all the experimental and numerical tests performed. The IR camera captured the temperature changes around the nostrils during breathing. The fluctuations in temperature caused by inspiration and expiration are illustrated in Figures 3(a) and 3(b), respectively. The Haar Cascade algorithm was implemented to automate the nasal ROI detection and tracking in the subject's thermal video. Once the nasal ROI was detected, the canny edge detector was employed to identify the ROM. The ROM, a secondary ROI within the nasal ROI, focuses on the nostril to enhance the accuracy of breathing signal extraction. Figure 4 presents examples of the detected ROI and ROM, as well as the system's tracking performance under various head movements.

Specifically, Figure 4(a) shows an example of the detected ROI and ROM on the face. Figures 4(b)-4(d) demonstrate the system's ability to track the ROI and ROM under various head movements. In Figure 4(b), accurate tracking is observed when the subject's head is in a neutral position. In Figure 4(c), the system successfully adjusts and continues tracking despite an upward movement. Figure 4(d) shows the system maintaining focus on the nose even during a head tilt, demonstrating robustness in challenging orientations. These results highlight the system's adaptability to head movements, ensuring reliable detection and tracking of breathing signals, which is essential for accurate non-contact BR monitoring.

These findings directly address gaps identified in previous research. Prior studies [7]-[21], required manual selection of the ROI in the initial frame and faced challenges during large or abrupt head movements, often resulting in zero-value breathing signals. Moreover, tracking algorithms from earlier works struggled with motion artifacts, which compromised the continuity and reliability of the breathing signal. In contrast, this study implements a fully automated approach using the Haar Cascade classifier for nasal ROI detection and the canny edge detector for nostril segmentation, enhancing accuracy and robustness. These improvements ensure consistent performance despite head movements, overcoming key limitations of previous methods.

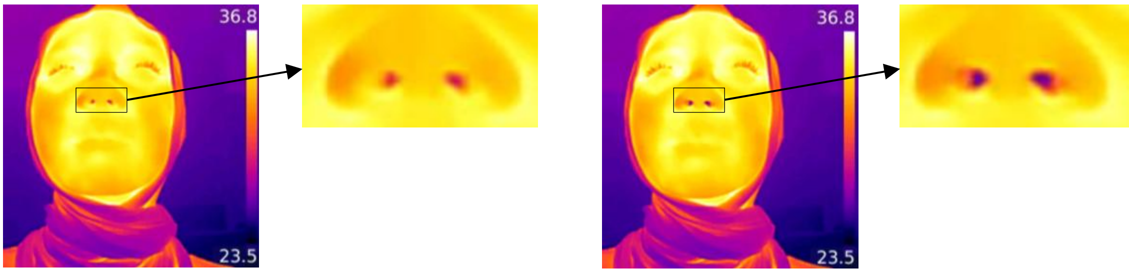

(a) (b)

Figure 3. Temperature variation around the nostrils during (a) inspiration and (b) expiration

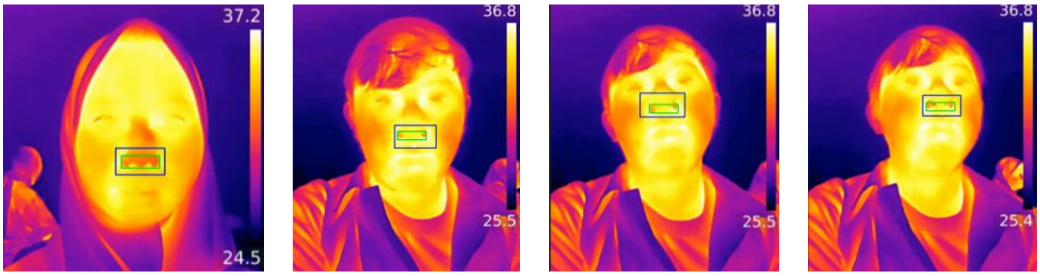

(a) (b) (c) (d)

Figure 4. ROI and ROM tracking: (a) detected in thermal video, (b) in a neutral head position, (c) during slight upward head movement, and (d) during head tilt to the side

While nostrils did not move out of the camera's view in this study, we incorporated a preventive interpolation step to address potential zero-value breathing signals that could arise in clinical settings. If nostril tracking were to fail, resulting in zero values, this algorithm would replace them with the average of surrounding data points. This approach fills in data gaps and smooths out abrupt signal jumps, helping maintain a continuous and consistent signal morphology. Consequently, the breathing signal remains reliable for further analysis, reducing the risk of misdetection from sudden zero-value interruptions. This interpolation method represents an innovative approach not addressed in prior studies, further bridging the identified research gap.

The extracted breathing signals generally exhibit low SNR. Hence, the signal was filtered using a second-order Butterworth bandpass filter, with a lower cutoff frequency set at 0.1 Hz and an upper cutoff of at 0.5 Hz. Figure 5 presents a comparison between the raw and filtered breathing signals extracted from thermal videos. Specifically, Figure 5(a) shows the raw breathing signals, while Figure 5(b) displays the signals after filtering. The Butterworth bandpass filter effectively reduced noise, resulting in smoother signals with more apparent periodic patterns, where inspiratory peaks and expiratory troughs are more easily identified. While there was a slight amplitude shift between the raw and filtered signals, this did not affect the accuracy of BR detection, as the filter preserved the signal morphology, ensuring peak and trough identification remained reliable. After that, peak detection algorithms were applied to identify the peak and valley in the breathing signal, indicating the breathing cycle's inspiration and expiration phases. One breathing cycle consists of one inspiration phase and one expiration phase, defined as the distance between consecutive peaks or consecutive valleys. Thus, the BR can be calculated by one minute's total number of breath cycles.

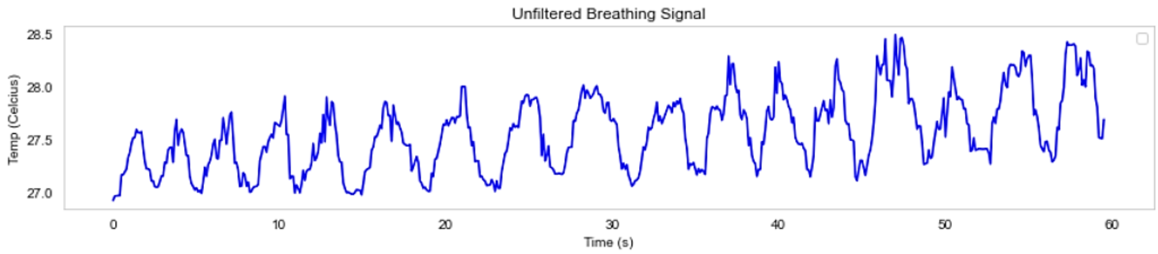

(a)

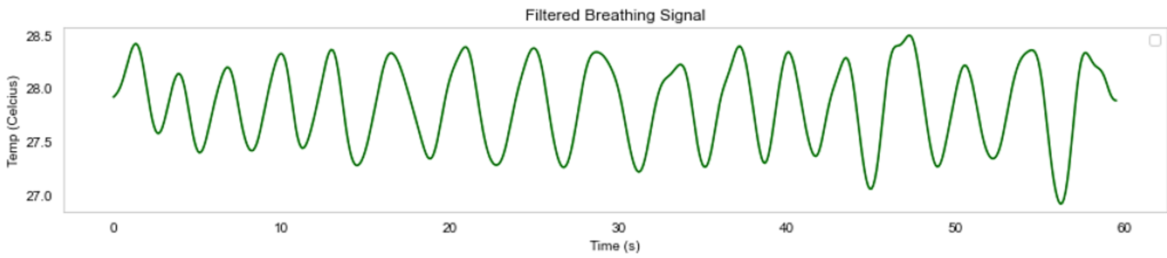

(b)

Figure 5. Extracted breathing signal (a) before filtering and (b) after filtering

3.1. Breathing rate calculation

This study evaluates respiratory rate estimation from thermal video recordings under three different conditions: (i) stationary normal breathing, (ii) head movement with normal breathing, and (iii) abnormal breathing patterns such as bradypnea or tachypnea.

Table 1 presents the performance of the proposed algorithm across these conditions. In condition 1 (C1), where subjects maintained a stationary posture while breathing normally, the algorithm demonstrated a high candidate index (CAND) of 94.57% on average, with values ranging from 91.03% to 99.65%. The mean absolute error (MAE) in respiratory rate estimation was 1.045 bpm, with the highest observed error at 1.77 bpm and the lowest at 0.07 bpm. These results indicate that the algorithm performs accurately under static conditions.

In condition 2 (C2), where subjects performed head movements while maintaining a normal breathing pattern, the algorithm remained robust, achieving an average CAND index of 93.71%, with values ranging from 87.31% to 99.77%. However, due to motion artifacts introduced by head movements, there was a slight increase in the MAE to 1.259 bpm. The highest individual error recorded in this condition was 2.73 bpm, while the lowest was 0.04 bpm. This suggests that while the method remains effective in dynamic settings, additional motion compensation techniques may be required to enhance accuracy.

In condition 3 (C3), which involved abnormal breathing patterns such as bradypnea and tachypnea, the algorithm maintained strong performance, achieving an average CAND index of 96.06%, with values ranging from 91.30% to 99.77%. The MAE was reduced to 0.607 bpm, with the highest error recorded at 1.23 bpm and the lowest at 0.04 bpm. These findings indicate that the proposed method is well-suited for detecting irregular respiratory patterns with high precision.

Overall, the results confirm that the proposed algorithm provides accurate respiratory rate estimation even under conditions involving motion artifacts and abnormal breathing patterns. The slight performance degradation observed in condition 2 (C2) suggests that further improvements in nasal tracking algorithms and motion compensation techniques could enhance robustness in dynamic environments. Future studies should focus on validating the method with a larger and more diverse dataset to strengthen its clinical applicability.

Table 1. Performance evaluation of system using CAND index and MAE

Subject	C1				C2				C3			
	RR_{GT} (bpm)	RR_{IRT} (bpm)	Error (bpm)	$CAND$ (%)	RR_{GT} (bpm)	RR_{IRT} (bpm)	Error (bpm)	$CAND$ (%)	RR_{GT} (bpm)	RR_{IRT} (bpm)	Error (bpm)	$CAND$ (%)
S1	21.93	23.36	1.43	93.48	17.13	18.47	1.34	92.18	24.83	25.64	0.81	96.74
S2	19.73	21.50	1.77	91.03	21.56	23.83	2.27	89.47	24.56	24.00	0.56	97.72
S3	17.50	17.05	0.45	97.43	17.83	19.52	1.69	90.52	9.48	9.00	0.48	94.94
S4	18.78	19.89	1.11	94.09	21.52	24.25	2.73	87.31	27.52	26.48	1.04	96.22
S5	21.87	23.07	1.20	94.51	20.43	21.35	0.92	95.49	10.95	11.00	0.05	99.54
S6	17.56	19.04	1.48	91.57	20.63	21.00	0.37	98.21	21.56	21.61	0.05	99.77
S7	20.13	21.20	0.07	99.65	20.52	21.42	0.90	95.61	10.12	11.00	0.88	91.30
S8	17.83	16.96	0.87	95.12	21.10	20.1	1.00	95.26	10.77	12.00	1.23	88.58
S9	18.98	20.58	1.60	91.57	19.85	18.52	1.33	93.29	10.16	10.33	0.17	98.33
S10	16.95	17.42	0.47	97.23	17.12	17.08	0.04	99.77	31.51	30.71	0.80	97.46
MEAN	**-**	**-**	**1.045**	**94.57**	**-**	**-**	**1.259**	**93.71**	**-**	**-**	**0.607**	**96.06**

3.2. Classification using k-NN

After calculating the BR, the k-NN classifier was employed to categorize the breathing signals into three conditions: tachypnea, normal, or bradypnea. Key features used for classification included the number of normal and abnormal cycles, as well as the calculated BR values. Breathing cycles were classified as normal if their duration ranged from 2.5 to 5 seconds per cycle; durations outside this range were considered abnormal. The k-NN classifier was trained using 416 breathing signals comprised 90 bradypnea, 200 normal breathing, and 126 tachypnea signals. The data was split into training and testing sets with a 7:3 ratio. To determine the optimal k value, validation accuracy was calculated for k values between 1 and 9, as shown in Figure 6. Based on Figure 6(a), the most effective k value is k=1, with the best validation accuracy of 100% and training accuracy of 100%. This indicates that the model can correctly classify the training data using the nearest neighbor.

With k=1 selected as the optimal value, the testing accuracy of the trained k-NN model was assessed, resulting in a testing accuracy of 99.2%. These results demonstrate the model's ability to maintain high accuracy on unseen data The confusion matrix generated by the k-NN classifier during testing is illustrated in Figure 6(b). The classifier's performance is further assessed by calculating each class's specificity, sensitivity, precision, and F1-score, as detailed in Table 2. These metrics offer insight into the model's accuracy in correctly identifying positive and negative classes. The results indicate that the k-NN model with the optimal k value is reliable for classification applications, demonstrating excellent performance in detecting and classifying data.

Our study focused on classifying three respiratory conditions-normal, bradypnea, and tachypnea-achieving higher accuracy than previous research, with 100% for training and validation, and 99.2% for testing. In contrast, prior work classified four conditions and reported accuracies of 98.59% (training), 99.5% (validation), and 98% (testing). Furthermore, our system was tested under three video data variations, including movement scenarios, demonstrating its robustness in dynamic environments. These results highlight the reliability and practical applicability of our non-contact BR monitoring approach.

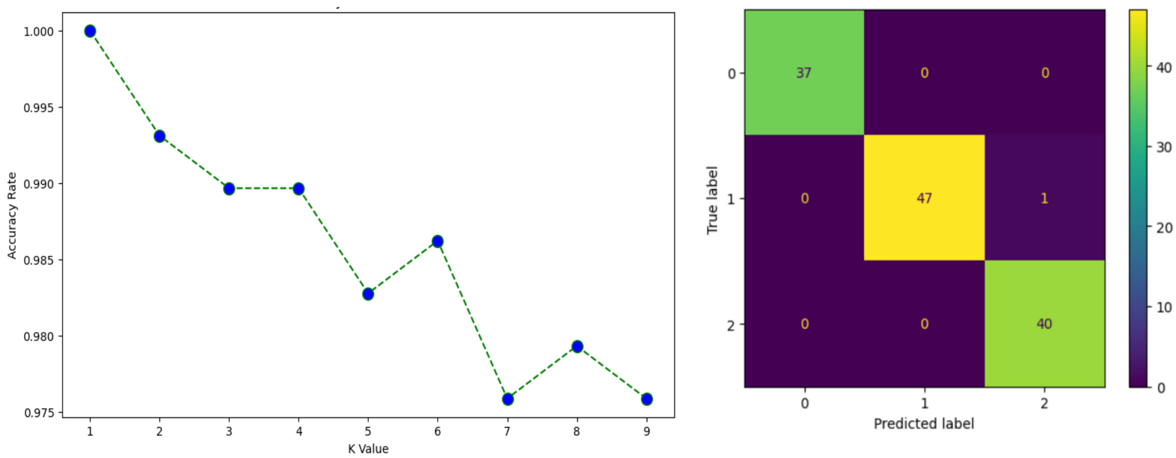

(a) (b)

Figure 6. Results showing (a) accuracy values from 10-fold cross-validation of the k-NN classifier across various k values, and (b) the confusion matrix generated by the k-NN classifier during testing with k=1

Table 2. Statistical evaluation of the 10-fold cross validation k-NN classifier for each class at k=1

Class	Spesificity	Sensitivity	Precision	F1-score
Bradypnea	1.00	1.00	1.00	1.00
Normal	1.00	0.9872	1.00	0.9936
Tachypnea	0.9882	1.00	0.9756	0.9876

4. CONCLUSION

This study presents a reliable non-contact system for monitoring respiratory rate using IRT. By tracking nasal temperature fluctuations during inspiration and expiration, the proposed method effectively estimates BR with high accuracy across different conditions. The integration of Haar Cascade, Canny edge detection, and a Butterworth bandpass filter enhances signal quality, while a k-NN classifier enables reliable classification of breathing patterns. Experimental results demonstrate the system's strong performance, achieving CAND indices of 94.57%, 93.71%, and 96.06% for stationary, moving, and abnormal breathing conditions, respectively, with low MAE. The k-NN classifier further validated its effectiveness with 99.2% accuracy in testing. These findings highlight the potential of IRT for non-invasive respiratory monitoring in clinical and home settings. Future work should focus on optimizing the algorithm for diverse patient populations and integrating the system into real-time healthcare frameworks for early detection of respiratory disorders.

FUNDING INFORMATION

This research was supported by the Department of Biomedical Engineering, Institut Teknologi Sepuluh Nopember (ITS), through the Biomedical Engineering ITS 2024 Research Funding (No. 969/PKS/ITS/2024).

AUTHOR CONTRIBUTIONS STATEMENT

Name of Author	C	M	So	Va	Fo	I	R	D	O	E	Vi	Su	P	Fu
Anadya Ghina Salsabila	✓	✓	✓		✓	✓		✓	✓	✓	✓		✓	
Rachmad Setiawan		✓		✓			✓	✓		✓		✓		✓
Nada Fitrieyatul Hikmah	✓	✓		✓			✓	✓		✓		✓	✓	✓
Zain Budi Syulthoni	✓			✓						✓		✓		

C : **C**onceptualization
M : **M**ethodology
So : **So**ftware
Va : **Va**lidation
Fo : **Fo**rmal analysis
I : **I**nvestigation
R : **R**esources
D : **D**ata Curation
O : Writing - **O**riginal Draft
E : Writing - Review & **E**diting
Vi : **Vi**sualization
Su : **Su**pervision
P : **P**roject administration
Fu : **Fu**nding acquisition

CONFLICT OF INTEREST STATEMENT

Authors state no conflict of interest.

INFORMED CONSENT

We have obtained informed consent from all individuals included in this study.

DATA AVAILABILITY

The data that support the findings of this study are available on request from the corresponding author, N.F.H. The data, which contain information that could compromise the privacy of research participants, are not publicly available due to certain restrictions.

REFERENCES

[1] D. D. Taralunga, B. Monacu, and R. Tapu, "Automatic real time derivation of breathing rate from thermal video sequences," *IFMBE Proceedings*, vol. 65, pp. 81-84, 2017, doi: 10.1007/978-981-10-5122-7_21.

[2] P. Jagadev and L. I. Giri, "Non-contact monitoring of human respiration using infrared thermography and machine learning," *Infrared Physics and Technology*, vol. 104, 2020, doi: 10.1016/j.infrared.2019.103117.

[3] D. C. J. Howell and L. Flower, "Signs of respiratory disease: Breathing patterns," *Encyclopedia of Respiratory Medicine*, pp. 53–56, 2022, doi: 10.1016/B0-12-370879-6%2F00352-5.

[4] C. B. Pereira, X. Yu1, M. Czaplik, V. Blazek, B. Venema, and S. Leonhardt, "Estimation of breathing rate in thermal imaging videos: a pilot study on healthy human subjects," *Journal of Clinical Monitoring and Computing*, vol. 31, pp. 1241-1254, 2017, doi: 10.1007/s10877-016-9949-y.

[5] C. B. Pereira, X. Yu1, M. Czaplik, V. Blazek, B. Venema, S. Leonhardt, and D. Teichmann, "Monitoring of cardiorespiratory signals using thermal imaging: a pilot study on healthy human subjects," *Sensors*, vol. 28, 2018, doi: 10.3390/s18051541.

[6] F. S. A. Resta, R. Setiawan, N. F. Hikmah, and R. Amalia, "Noncontact electrocardiogram system for mattresses using silver conductive fabric," in *11th International Conference on Electrical Engineering, Computer Science and Informatics*, pp. 33-38, 2024, doi: 10.1109/EECSI63442.2024.10776162.

[7] J. Fei and I. Pavlidis, "Thermistor at a distance: unobtrusive measurement of breathing," *IEEE Transactions on Biomedical Engineering*, vol. 57, no. 4, pp. 988–998, 2010, doi: 10.1109/TBME.2009.2032415.

[8] N. F. Hikmah, R. Setiawan, and M. D. Gunawan, "Sleep quality assessment from robust heart and muscle fatigue estimation using supervised machine learning," *International Journal of Intelligent Engineering and Systems*, vol. 16, no. 2, pp. 319-331, 2023, doi: 10.22266/ijies2023.0430.26.

[9] R. Murthy, I. Pavlidis, and P. Tsiamyrtzis, "Touchless monitoring of breathing function," in *Proceedings of IEEE Engineering in Medicine and Biology Society* (IEEE, 2004), pp. 1196–1199, doi: 10.1109/IEMBS.2004.1403382.

[10] R. G. Soto, E. S. Fu, H. Vila, and R. V. Miguel, "Capnography accurately detects apnea during monitored anes thesia care," *Anesth. Analg.*, vol. 99, no. 2, pp. 379–382, 2004, doi: 10.1213/01.ANE.0000131964.67524.E7.

[11] L. Mauryaa, P. Mahapatrab, and D. Chawla, "Non-contact breathing monitoring by integrating RGB and thermal imaging via RGB-thermal image registration," *Biocybernetics and Biomedical Engineering*, vol. 41, pp. 1107-1122, 2021, doi: 10.1016/j.bbe.2021.07.002.

[12] C. B. Pereira, X. Yu1, M. Czaplik, V. Blazek, B. Venema, and S. Leonhardt, "Remote monitoring of breathing dynamics using infrared thermography," *Biomedical Optics Express*, vol. 6, pp. 4378–4394, 2015, doi: 10.1364/BOE.6.004378.

[13] A. D. Droitcour *et al.*, "Non-contact respiratory rate measurement validation for hospitalized patients," In *Proceedings of the IEEE Engineering in Medicine and Biology Society*, Minneapolis, MN, USA, 2–6 September 2009; pp. 4812–4815, doi: 10.1109/IEMBS.2009.5332635.

[14] D. Shao, Y. Yang, C. Liu, F. Tsow, H. Yu, and N. Tao, "Non contact monitoring breathing pattern, exhalation flow rate and pulse transit time," *IEEE Transactions on Biomedical Engineering*, vol. 61, no. 11, pp. 2760–2767, 2014, doi: 10.1109/TBME.2014.2327024.

[15] A. D. Sanjaya, R. Setiawan, and N. F. Hikmah, "RNA-BioLens: a novel raspberry pi-based digital microscope with image processing for acute lymphoblastic leukemia detection," in *IEEE Access*, vol. 13, pp. 23618-23628, 2025, doi: 10.1109/ACCESS.2025.3532305.

[16] A. K. Abbas, K. Heimann, K. Jergus, T. Orlikowsky, and S. Leonhardt, "Neonatal non-contact respiratory monitoring based on real-time infrared thermography," *BioMedical Engineering OnLine*, vol. 10, no. 93, 2011, doi: 10.1186/1475-925X-10-93.

[17] M. C. T. Manullang, Y.-H. Lin, S.-J. Lai, and N.-K. Chou, "Implementation of thermal camera for non-contact physiological measurement: a systematic review," *Sensors*, vol. 21, no. 7777, 2021, doi: 10.3390/s21237777.

[18] P. Battalwar, J. Gokhale, and U. Bansod, "Infrared thermography and IR camera," *History 1*, vol. 2, 2015.

[19] M. F. M. Shakhih, A. A. Wahab, and M. I. M. Salim, "Assessment of inspiration and expiration time using infrared thermal imaging modality," *Infrared Physics and Technology*, vol. 99, pp. 129-139, 2019, doi: 10.1016/j.infrared.2019.04.012.

[20] G. F. Lewis, R. G. Gatto, and S. W. Porges, "A novel method for extracting respiration rate and relative tidal volume from infrared thermography," *Psychophysiology*, vol. 48, no. 7, pp. 877–887, 2011, doi: 10.1111/j.1469-8986.2010.01167.x.

[21] R. Chauvin, M. Hamel, S. Bri`ere, F. Ferland, F. Grondin, D. L´etourneau, M. Tousignant, and F. Michaud, "Contact-free respiration rate monitoring using a pan-tilt thermal camera for stationary bike telerehabilitation sessions," *IEEE Systems Journal*, 2014, doi: 10.1109/JSYST.2014.2336372.

[22] UTI260B Thermal Camera, Uni-T, [Online]. Available: https://thermal.uni-trend.com/product/uti260b/ (accessed on July 2, 2024)

[23] A. C. D. Rahajeng, M. Nuh and N. F. Hikmah, "An evaluation performance of kernel on support vector machine to classify the skin tumors in dermoscopy image," *2020 International Conference on Computer Engineering, Network, and Intelligent Multimedia (CENIM)*, Surabaya, Indonesia, 2020, pp. 76-81, doi: 10.1109/CENIM51130.2020.9297941.

[24] F. G. Nabi, K. Sundaraj, M. S. Iqbal, M. Shafiq, and R. Palaniappan, "A telemedicine software application for asthma severity levels identification using wheeze sounds classification," *Biocybernetics and Bioengineering*, vol. 42, pp. 1236-1247, 2022, doi: 10.1016/j.bbe.2022.11.001.

[25] S. Hashim and P. Mccullagh, "Face detection by using haar cascade classifier," *Wasit Journal of Computer and Mathematics Science*, vol. 2. pp. 1-8, 2023, doi: 10.31185/wjcm.109.

[26] C. H. Setjo, B. Achmad, and Faridah, "Thermal image human detection using haar cascade classifier," *In 7th International Annual Engineering Seminar (InAES)*, Yogyakarta, Indonesia, 2017, doi: 10.1109/INAES.2017.8068554.

[27] M. D. Gunawan, R. Setiawan and N. F. Hikmah, "Estimation of sleep quality based on HRV, EMG, and EEG parameters with K-nearest neighbor method," *2024 International Seminar on Intelligent Technology and Its Applications (ISITIA)*, Mataram, Indonesia, 2024, pp. 651-656, doi: 10.1109/ISITIA63062.2024.10668227.

[28] M. A. F. Pimentel *et al.*, "Towards robust estimation of respiratory rate from pulse oximeters," *IEEE Transactions on Biomedical Engineering*, vol. 64, no. 8, pp. 1914-1923, 2016, doi: 10.1109/TBME.2016.2613124.

[29] L. Wimmert, "Respiratory signal database," GitHub, 2024. [Online]. Available: https://github.com/IPMI-ICNS-UKE/respiratory-signal-database?tab=readme-ov-file. (Accessed on July 1, 2024.)

BIOGRAPHIES OF AUTHORS

Anadya Ghina Salsabila earned her bachelor's degree in Biomedical Engineering from Institut Teknologi Sepuluh Nopember (ITS), Surabaya, Indonesia in 2024. She has a strong interest in medical imaging and human signal processing. Her research focuses on monitoring human vital signs using infrared thermography and machine learning, with a particular emphasis on human breathing rate. She has also worked on research involving the detection of multiple vital signs, including breathing rate, heart rate, and body temperature, using thermal imaging. For further communication or inquiries. She can be contacted at anadyaghina@gmail.com.

Rachmad Setiawan earned a bachelor's degree in Electronics from Institut Teknologi Sepuluh Nopember (ITS) in 1995. Then continued his Masters degree in Instrumentation and Control at Institut Teknologi Bandung (ITB), and earned his Master's degree in 1999. In 2013-2014 he conducted researched the development of closed-loop fes system, with an emphasis on developing system infrastructure, joint angle sensors, and wearable controllers based on wireless technology. His current activity is to become a lecturer at the Department of Biomedical Engineering, Faculty of Intelligent Electrical Technology and Informatics, Institut Teknologi Sepuluh Nopember (ITS), Indonesia. He can be contacted at email: rachmad@bme.its.ac.id.

Nada Fitrieyatul Hikmah S.T., M.T. is a lecturer and has been serving as the Secretary of the Department of Biomedical Engineering at Institut Teknologi Sepuluh Nopember (ITS), Indonesia, since 2025. She earned her Bachelor's degree in Biomedical Engineering from Universitas Airlangga (UNAIR) in 2012 and her Master's degree in Electrical Engineering – Electronics, specializing in Biomedical Engineering, from ITS in 2016. Her research interests include cardiac engineering, biomedical signal processing, and medical imaging, with a focus on developing advanced technologies for healthcare applications. Throughout her academic career, she has been actively involved in research collaborations, scientific publications, and student mentoring. She can be contacted via email at nadafh@bme.its.ac.id.

dr. Zain Budi Syulthoni, Sp.K.J. earned his Medical Doctor in Faculty of Medicine from Universitas Airlangga (UNAIR) in 2010 and his Psychiatrist Specialist at Universitas Airlangga (UNAIR) in 2021. Currently, he works as a lecturer at the Faculty of Medicine and Health, Institut Teknologi Sepuluh Nopember (ITS), Indonesia. His research interests include early intervention in psychiatric disorders, child and adolescent psychiatric, technology-based intervention in psychiatric. He can be contacted at email: zain.budi@its.ac.id.